A00-16524

AIAA 2000-0664

Mach Number Effects on Entrainment and Mixing in Supersonic Planar Turbulent Wakes

Masaki Nakagawa and Werner J.A. Dahm

Laboratory for Turbulence and Combustion (LTC)
Department of Aerospace Engineering
The University of Michigan
Ann Arbor, MI

38th Aerospace Sciences Meeting & Exhibit
10-13 January 2000 / Reno, NV

AIAA Paper No. 2000-0664 presented at the 38th AIAA Aerospace Sciences Meeting and Exhibit, 10-13 January 2000, Reno, NV.

Mach Number Effects on Entrainment and Mixing in Supersonic Planar Turbulent Wakes

Masaki Nakagawa[1] and Werner J.A. Dahm[2]

Laboratory for Turbulence and Combustion (LTC)
Department of Aerospace Engineering
The University of Michigan
Ann Arbor, MI 48109-2140

Results are presented from an experimental investigation of Mach number effects on entrainment and mixing in a supersonic, planar, turbulent, bluff-body wake formed by a two-dimensional slot jet nozzle aligned with two different Mach number free stream produced by Mach 2.0 and Mach 3.0 nozzles. Planar laser Mie scattering (PLMS) and shadowgraph imaging are combined with pitot and static pressure measurements to examine the mean flow scaling laws and the instantaneous structure of the flow fields. Results for both flows show classical vortex street-like large-scale structures in the wake far field, where the relative Mach numbers have decreased to clearly subsonic values, and the growth rates and velocity decays in the near field followed the characteristic $(\delta/\vartheta) \sim (x/\vartheta)^{1/2}$ and $(u/U) \sim (x/\vartheta)^{-1/2}$ scaling of incompressible planar turbulent wakes. These scaling constants agreed with values for forced incompressible wakes for the Mach 2 case, while those for the Mach 3 case agreed with unforced values, presumably due to the potential existence of "subsonic path". Moreover the interaction of reflected expansion waves with the large-scale vortical structures in the wake appeared to increase the growth rate drastically for both flows which may be attributable to its "self-exited forcing mechanism".

1. INTRODUCTION

Supersonic combustion has been an important research area in the last few decades of the 20th century to develop the next generation airbreathing propulsion systems. These systems may involve combustors, in which a subsonic fuel stream must be mixed and burned with a supersonic air stream. Under such conditions, compressibility effects can significantly alter the entrainment and mixing processes from prior design experience in subsonic flows. Many research efforts have been undertaken in order to establish the technical background to develop such supersonic combustors.

Over the past decade, intensive fundamental research work has been conducted to clarify the effects of compressibility on turbulent shear flows, especially for experimental and numerical research on supersonic mixing layer. These have shown the major effects of compressibility to be a reduction in the growth rate and loss of two dimensionality in the large-scale structure (*e.g.*, Clemens & Mungal 1995). These effects are widely believed to be generic to all supersonic turbulent shear flows. However, other shear flows with other scaling properties, and therefore other large-scale structure characteristics, may also show certain other phenomena which are not present in mixing layers.

From this motivation, our previous experimental investigation (Nakagawa & Dahm 1999) focused primarily on visualization results for the instantaneous large scale structure and mean scaling properties of two-dimensional, supersonic, turbulent, bluff-body wakes, and made comparisons with incompressible turbulent wakes. The results showed a classical vortex street-like large-scale structure in the wake far field, where the relative Mach number has decreased to clearly subsonic values. Where the relative Mach number is transonic, the far-field growth rate and velocity decay followed the characteristic $(\delta/\vartheta) \sim (x/\vartheta)^{1/2}$ and $(u/U) \sim (x/\vartheta)^{-1/2}$ scaling of incompressible planar turbulent wakes. The interaction of the reflected expansion wave with the large-scale vortical structures in the wake appeared to produce quasi-periodic forcing that affects the constants in scaling of the local flow width and velocity defect.

In this paper we present results from an experimental investigation into the effects of Mach number on the large-scale structure and associated entrainment and mixing properties of supersonic planar turbulent wakes with two different Mach number free streams. These are compared with the results from incompressible planar turbulent wakes and corresponding results in the supersonic turbulent mixing layer in order to clarify the mechanism of such phenomena as seen in the previous work and ultimately, the generic effects of compressibility on turbulent shear flows.

2. FACILITY AND DIAGNOSTICS

The experiments reported here were conducted in a Supersonic Mixing and Combustion Flow Facility designed specifically for studies of supersonic coflowing turbulent jets and wakes. The test section interior measured 34.6 mm × 38.4 mm in cross section and 553 mm in length. A subsonic slot nozzle having exterior dimensions of 4.2 mm × 38.4 mm and interior dimensions of 2.0 mm × 36.2 mm was centered in the test section entrance plane. The slot nozzle entered the tunnel through a 1/4-in. ID round tube, and then flattened in the lateral direction just upstream of the throat while expanding in the spanwise direction. The nozzle was packed with glass beads and screens immediately after the expansion section and through most of the parallel section to give a uniform low-speed flow

[1] Graduate Student; AIAA Student Member.
[2] Professor; AIAA Senior Member; Corresponding author.

(typically 50 to 100 m/s) across the exit plane of the slot. The present results are for air flow through the slot nozzle, in some cases with alcohol vapor seeding for visualization purposes.

The supersonic nozzles were designed, with dimensions summarized in Table 1, using the NOZCS3 program from the University of Illinois to produce wave-free Mach 2.0 and Mach 3.0 airflow in the presence of the slot nozzle. However, owing to the relatively small cross section of the tunnel, viscous boundary layers along the supersonic nozzle and tunnel sidewalls, and along the outer walls of the slot nozzles, produced a reduction in the effective cross sectional area of the tunnel. Therefore nominal Mach numbers in each of the two free streams are lower than the design values. However, for simplicity we refer to these as the Mach 2 case, and the Mach 3 case, respectively.

The wall static pressure distribution was monitored with 16 sidewall pressure taps on each side. Sidewalls were kept parallel for all results reported here. Any variations in wall static pressure due to the displacement effect of the wake flow itself were negligible in comparison with variations induced by the repeated reflections of the wake expansion fan and recompression shock from the tunnel walls. Static pressures were measured on the centerline of the test section with 30 pressure taps on both front and back sides of the wall. Pitot pressures were measured across the flow at many downstream locations with probes designed as recommended by Pope & Goin (1965). Pitot pressure data were converted to Mach number combined with static pressure at each location using the Rayleigh supersonic pitot formula.

Schlieren and shadowgraph imaging were used to document the wave patterns throughout the test section. Light from a Xenon Corp. Nanolamp with 20 nsec pulse duration passed through a microscope objective with a 400 μm pinhole and was imaged onto a Princeton Instruments thermoelectrically cooled 576 × 384 CCD array.

M_{design}	2.0		3.0	
A^*	8.99 mm × 38.4 mm		3.58 mm × 38.4 mm	
A_{exit}	15.2 mm × 38.4 mm		15.2 mm × 38.4 mm	
L	63.5 mm		71.12 mm	
M_{exit}	1.86	1.73	2.66	2.57
U_{exit}	482 m/s	461m/s	577 m/s	569 m/s
T_{exit}	167 K	177 K	117 K	122 K
Re_L	2.1 × 10⁶		2.9 × 10⁶	
ϑ	0.4 mm		0.55 mm	
Re_ϑ	31,000		23,000	

A^* : Nozzle throat area;
L : Distance from nozzle throat to nozzle exit;
Re_ϑ: Wake Reynolds number considering temperature and pressure effects

Table 1. Summary of dimensions of supersonic nozzles and experimental conditions with associated flow parameters.

Planar laser Mie scattering (PLMS) imaging was used to document the instantaneous structure and growth rate of the flow. Alcohol vapor was introduced into the air issuing from the slot nozzle by spraying ethanol into a heated seeder located approximately 1 m upstream of the nozzle. Uniformly mixed alcohol vaporizes in the air stream before exiting the nozzle, with the resulting mass fraction of alcohol being very small (0.85 to 2 ml/sec) which is enough for the alcohol particles to follow the turbulent flow motion. When the alcohol vapor mixes with the cold, supersonic, free stream air in the test section, it condenses to form a fine fog. A thin laser sheet formed from an Nd:YAG laser, with a wavelength of 532 nm and 10 nsec pulse duration, passes through the wake, and Mie scattering from the fog is imaged onto a 512 × 512 CCD array. Details of schematics of the test section and imaging systems are shown in our previous paper (Nakagawa & Dahm 1999).

3. FLOW VISUALIZATION RESULTS

3.1. Instantaneous PLMS Images

Figure 1 shows three typical examples of the resulting instantaneous PLMS images for the Mach 2 and Mach 3 cases, spanning from the nozzle exit well into the wake far field. The comparatively steady base flow region can be seen at the extreme left side of these images in Fig. 1*a*. At about x = 3 cm downstream of the jet nozzle (*i.e.*, around $x/\vartheta \approx 75$), large-scale organized vortical structures with alternating signs of circulation can be seen to begin forming. By about x = 6 cm, corresponding to $x/\vartheta \approx 150$, these structures typically have organized into a characteristic, quasi-periodic, vortex street-like pattern that continues downstream. The wake can be seen to broaden slowly with increasing downstream distance. The size and spacing of the vortical structures appears to increase with the width of the wake.

For the Mach 3 case in Fig. 1b, the alcohol seeding level must be kept lower to avoid forming large droplets due to the lower free stream temperature. As a consequence, PLMS visualization is not possible until about x = 3 cm. At about x = 4 cm downstream of the jet nozzle (*i.e.*, around $x/\vartheta \approx 75$), large-scale organized vortical structures can be seen to begin forming. By about x = 6 cm, corresponding to $x/\vartheta \approx 100$, these structures have organized into a similar vortex street-like pattern as seen in the Mach 2 case.

3.2. Ensemble Averaged PLMS Images

Figure 2 shows the ensemble-average of 80 instantaneous PLMS images of the type in Fig. 1, combined with typical shadowgraph images of flows on each of which the mean PLMS image is superimposed for comparison. The mean growth of the wake can be readily seen in Fig. 2*a* for the Mach 2 case. The slightly darker regions near x/ϑ = 180 and 330 coincide with interactions between the flow and reflections of the wake shock (recompression wave) from the tunnel sidewalls. The wake is also deflected slightly after each of these shock interactions, due to the small asymmetry in the shock reflections caused by the slight mismatch in Mach numbers entering the test section on either side of the jet nozzle. This slight asymmetry in the shock pattern can be seen in the shadowgraph image.

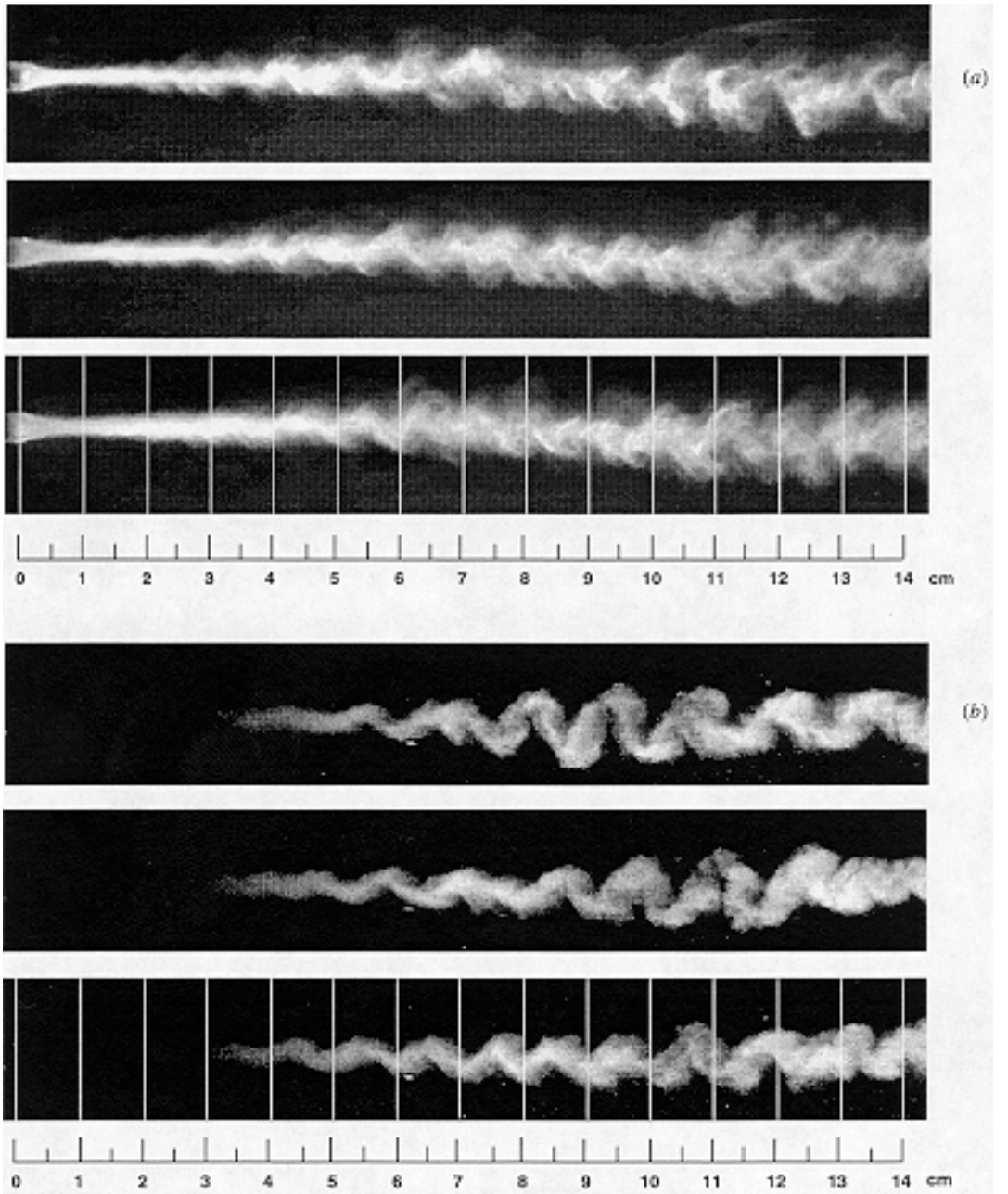

Figure 1. Typical instantaneous PLMS images for (*a*) Mach 2 case and (*b*) Mach 3 case, showing structures in the supersonic, planar, turbulent wake flow. Note development of characteristic vortex street-like large scale structures in far field, with alternating signs of circulation, and the lack of any apparent structures immediately downstream of base flow region, where the relative Mach number remains high.

The slightly darker region for the Mach 3 case in Fig. 2*b* also coincides with interactions between the flow and reflections of the recompression wave near $x/\vartheta = 200$. In this higher Mach number case, free stream shock intersection can be seen in the mean PLMS image. The angles of the expansion and the compression waves created in the base flow region become shallower, and consequently the reflected waves intersect further downstream than in the Mach 2 case.

3.3. Pitot Pressure Profiles

Pitot pressure profiles were measured for each free stream Mach number. Figure 3 shows typical profiles taken at the first eight of a total of 16 downstream locations for the Mach 2 case, superimposed on a shadowgraph image to allow the wave structure to be reconciled with the pressure profiles. Pressures were measured in the transverse direction with a 0.5 mm increment at each downstream location. The extent of the expansion fan and the point where the trailing Mach wave

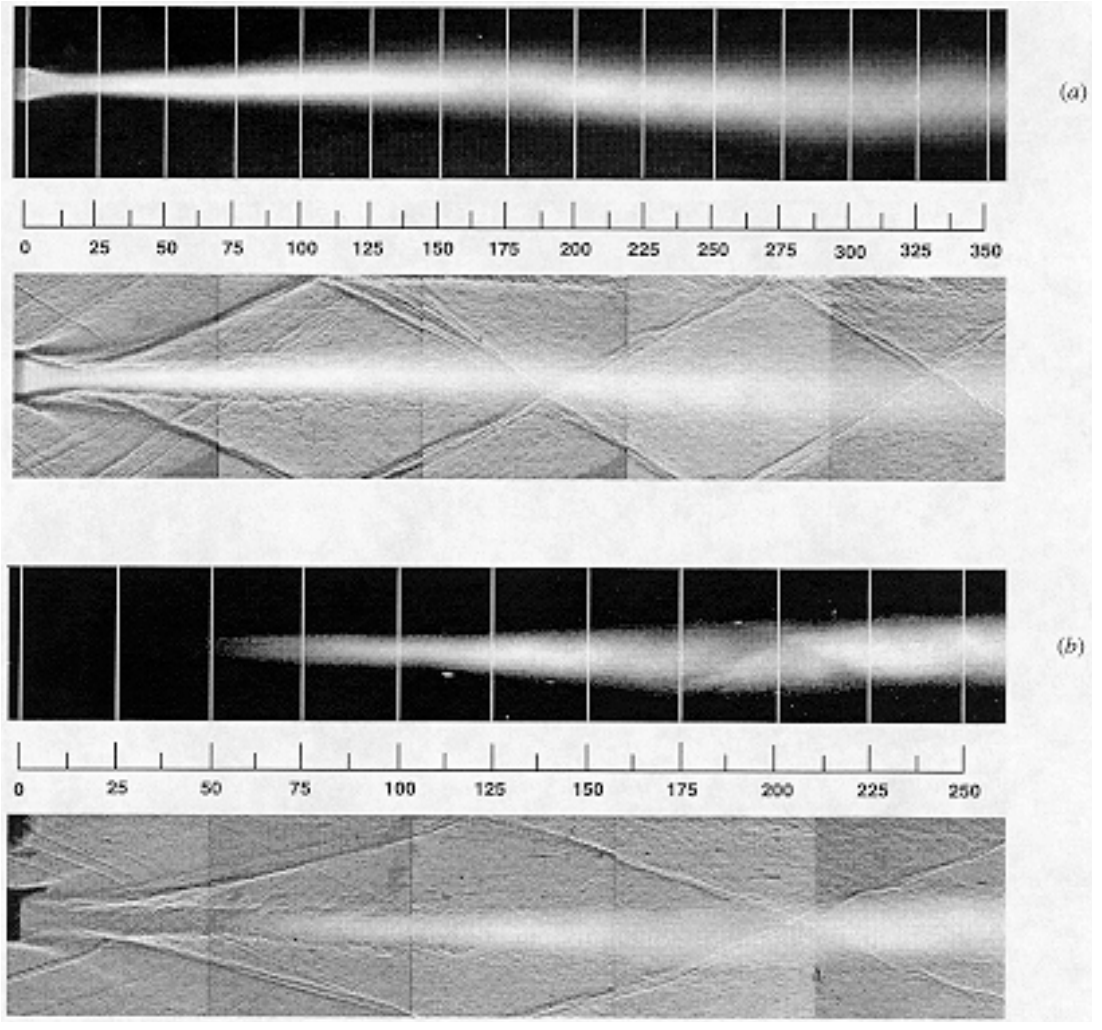

Figure 2. Ensemble-averaged PLMS image for the supersonic, planar, turbulent wake flow *(top)* and instantaneous shadowgraph image, showing wave structure for parallel sidewalls, with mean PLMS image superimposed *(bottom)* for (*a*) the Mach 2 case and (*b*) the Mach 3 case. Scales give the distance from the jet nozzles in (x/ϑ). The angles of the expansion and the compression waves created in the base flow region become shallower, and consequently the reflected waves intersect further downstream than in the Mach 2 case.

intersects the recompression shock can be readily seen. Similar pitot pressure profiles in the wake region were measured for the Mach 3 case at 16 different downstream locations into the far field, at every 0.25 mm of the lateral position at each downstream location.

These results are used to determine the local Mach number and similarity scaling in §4 and also used in §5 to compare the scaling properties of the supersonic wake with results for incompressible wakes.

4. SIMILARITY SCALING

4.1 Similarity Profiles

The mean pitot pressure profiles such as in Fig. 3 at all 16 downstream locations were, combined with the corresponding static pressures, each converted to local Mach number M(y). These are then converted to mean velocity profiles $U(y)$ assuming adiabatic flow and subsequently to mean velocity defect profiles $u(y) = U - U(y)$. A Gaussian fit was determined for each $u(y)$ profile by matching the three lowest moments over the central portion of the flow spanning across the wake, allowing the local centerline location $y_0(x)$, local centerline velocity defect $u_0(x)$, and local flow width $\delta_{1/2}(x)$ of each profile to be found. Here $\delta_{1/2}(x)$ denotes the half-width at the half-maximum point of the local mean velocity defect profile.

Each of the measured velocity defect profiles $u(y)$, normalized by the local centerline velocity defect $u_0(x)$, with y centered on $y_0(x)$ and normalized by $\delta_{1/2}(x)$, is shown in Fig. 4 for each Mach number. It is apparent that except for the first few points all of the mean velocity defect profiles are nearly self-similar. The local wake momentum thickness $\vartheta(x)$, determined by appropriately integrating each of these $u(y)$ profiles, is essentially invariant with downstream distance x, yielding $\vartheta(x) \approx 0.40$ mm for the Mach 2 case and 0.55 mm for the Mach 3 case.

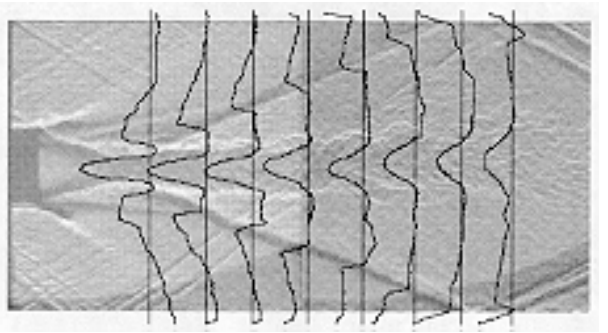

Figure 3. Measured total pressure profiles superimposed on shadowgraph for the Mach 2 case, showing relation between wave pattern and pitot pressure. Similar results were obtained for the Mach 3 case.

4.2 Relative Mach Number $M_r(x)$

Unlike the mixing layer or the wake created by a thin splitter plate, which does not produce strong waves, the bluff-body wake inherently produces a corner expansion wave and recompression shock. Reflections of these waves from the tunnel sidewalls thus inherently lead to Mach number variations in the free stream, and a single "free stream Mach number M " can thus not be defined. Figure 5 shows the resulting free stream Mach numbers M (x) immediately outside the flow on either side of the wake, determined from the measured pitot pressure profiles in Fig. 3, and the static pressures measured on the centerline of the test section for each case.

For the Mach 2 case the Mach number entering the test section on either side of the slot nozzle was M = 1.86 and 1.73, as in Table 1. As seen in Fig. 5*a*, the free streams are accelerated first by the expansion wave created at the corner of the slot nozzle, and then decrease to around 1.6 after passing through the compression wave. Thereafter M (x) gradually increases again up to 1.8 by passing through the reflected expansion waves, until reaching the reflected recompression wave around x = 4.75 cm or $(x/\vartheta) = 118$. For the Mach 3 case the free stream Mach numbers entering the test section are M = 2.66 and 2.57. Figure 5*b* shows similar variations as the free streams passing through the pattern of expansion and compression waves.

The relative Mach number $M_r(x) \equiv u_0(x)/a$ determined by the mean centerline velocity defect serves a corresponding role in the supersonic wake as does the convective Mach number M_c in the supersonic mixing layer. Moreover unlike the mixing layer, for which M_c does not vary with downstream distance x, the velocity defect in the wake must decrease with increasing x, and thus the relative Mach number $M_r(x)$ must also decrease with x.

Figure 6 shows the resulting relative Mach number M_r at each location (x/ϑ), from the measured centerline velocity defects $u_0(x)$ in Fig. 4 and M (x) in Fig. 5. It is apparent that $M_r(x)$ decreases rapidly, and that most of the far wake is at essentially incompressible local flow conditions for both flows. However in the supersonic turbulent mixing layer, reductions in the layer growth rate $d\delta/dx$ of more than 20% relative to the incompressible mixing layer are observed even at convective Mach numbers as low as 0.2. This suggests that, if observations in supersonic mixing layers were indeed indicative of generic effects of compressibility in other turbulent shear flows, then measurable compressibility effects should be expected up to at least $(x/\vartheta) = 100$ for the Mach 2 case and 150 for the Mach 3 case.

5. INCOMPRESSIBLE WAKE COMPARISONS

To look for effects of compressibility in the supersonic wake analogous to those observed in supersonic mixing layers, we compare the local outer variable scalings $\delta_{1/2}(x)$ and $u_0(x)$ to corresponding results from incompressible, planar, turbulent wakes. These outer variable scalings determine the local entrainment rate into the wake, and since at large values of the

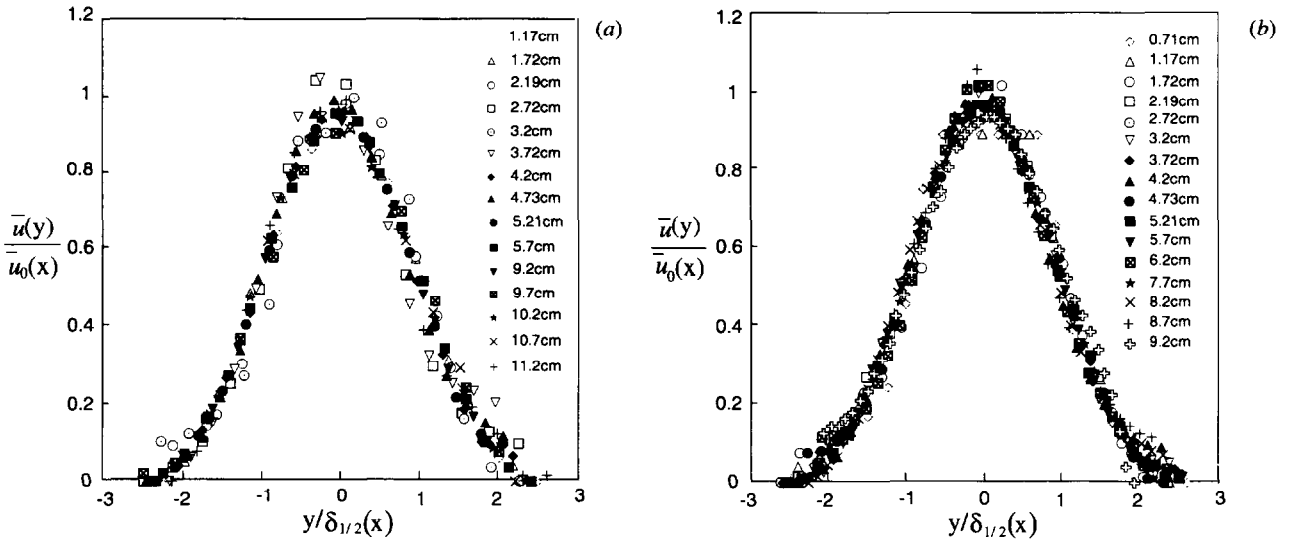

Figure 4. Similarity of measured mean velocity profiles for (*a*) the Mach 2 case and (*b*) the Mach 3 case, showing good collapse of all profiles except at the few points.

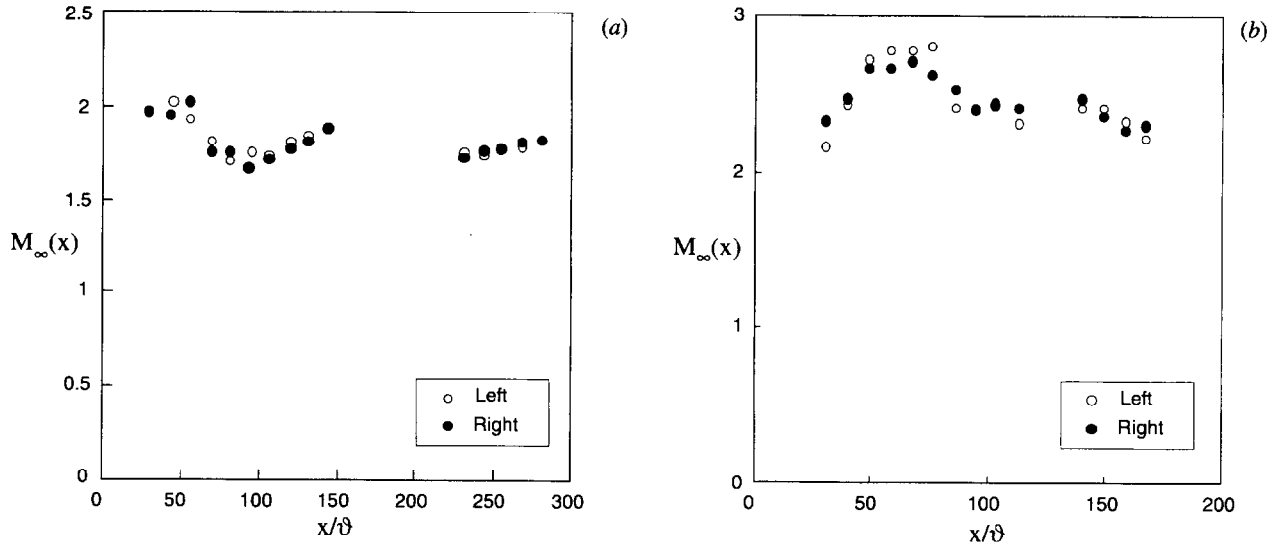

Figure 5. Free stream Mach number M (x) outside the wake for (a) Mach 2 case and (b) Mach 3 case.

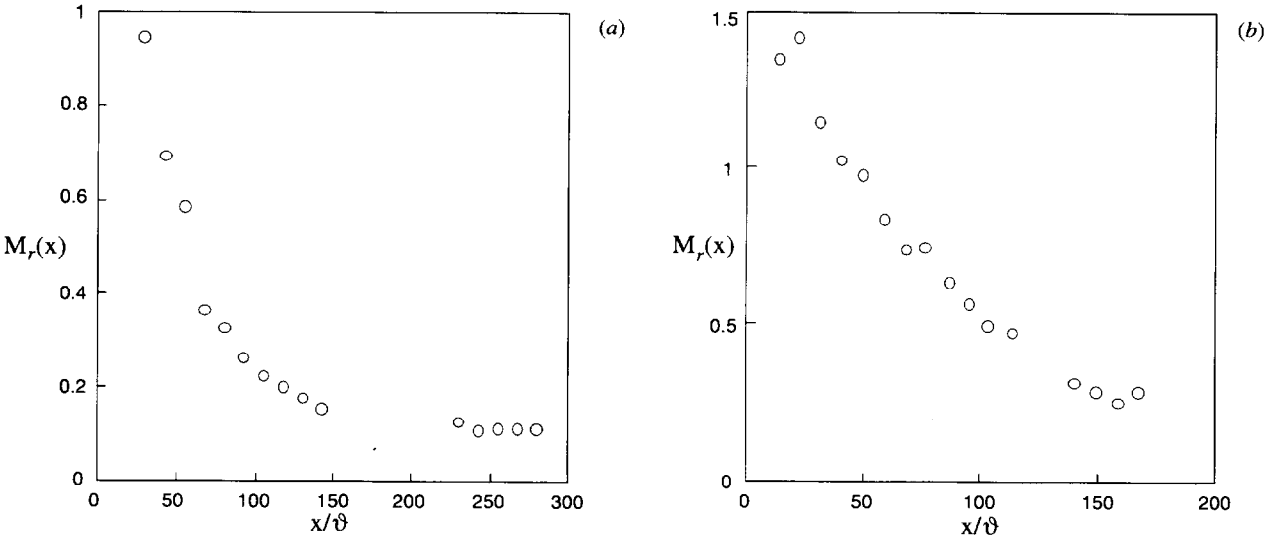

Figure 6. Relative Mach number $M_r(x)$ for (*a*) Mach 2 case and (*b*) Mach 3 case, determined from pressure ratios measured on the centerline at various downstream locations.

local outer-scale Reynolds number $Re_\delta(x) \equiv u_0(x) \cdot \delta_{1/2}(x)/\nu$ the molecular mixing rate is entrainment-limited, these scalings also determine the mixing rate achieved by the flow.

In incompressible planar turbulent wakes, the outer variable scalings in the self-similar far field have been relatively well established (*e.g.*, Wygnanski *et al* 1986). In particular, the flow width scales with the wake momentum thickness as

$$(\delta_{1/2}/\vartheta) = c_\delta\,[(x-x_0)/\vartheta]^{1/2}, \qquad (1)$$

and the centerline velocity defect scales as

$$(u/U_\infty) = c_u\,[(x-x_0)/\vartheta]^{-1/2}. \qquad (2)$$

The scaling constants c_δ and c_u, and the virtual origin x_0, depend on the wake generator. For bluff-body wakes, Wygnanski *et al* (1986) find

$$c_\delta = 0.270, \qquad (3a)$$

$$c_u = 1.88, \qquad (3b)$$

and

$$(x_0/\vartheta) = -128. \qquad (4)$$

For later reference, various other steady wake generators give $c_\delta = 0.29 \pm 0.03$ and $c_u = 1.70 \pm 0.2$. It is of interest to compare these power-law scalings and the constants for incompressible wakes with the present results for the supersonic wake.

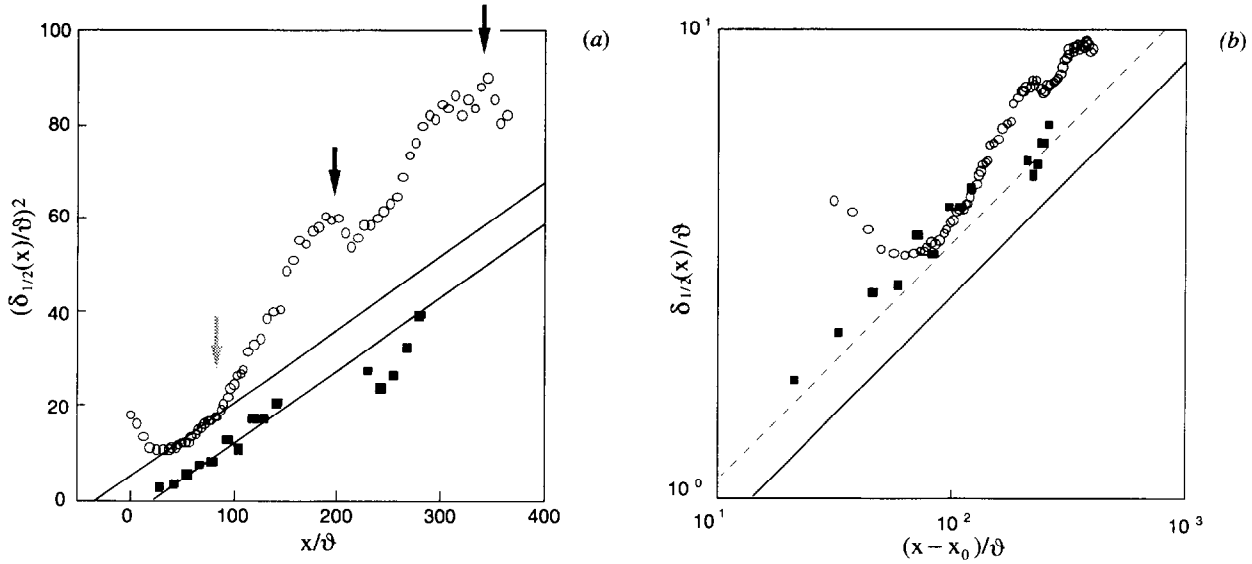

Figure 7. (*a*) Measured flow width $\delta_{1/2}(x)$ for the Mach 2 case from mean PLMS intensity profiles in Fig. 2*a* *(circles)* and from mean velocity profiles in Fig. 4*a* *(squares)*. Straight lines show $(\delta/\vartheta) \sim (x/\vartheta)^{1/2}$ scaling, and allow virtual origins and scaling constants to be determined. Profiles are accelerated around $(x/\vartheta) = 80$. Peaks of the growth rate at two locations near $(x/\vartheta) = 180$ and 330 coincide with locations of recompression wave intersections in Fig. 2*a*, as indicated by black arrows. The gray arrow indicates the point where the leading characteristics of expansion wave intersects on the center. (*b*) Flow widths $\delta_{1/2}(x)$ from Fig. 7*a* in log-log form, with lines indicating 1/2-power law scaling for values of the far-field scaling constant c_δ in (1) for forced incompressible wakes *(dashed line)* and unforced incompressible wakes *(solid line)* of Wygnanski *et al* (1986).

5.1 Flow Width Scaling $\delta(x)$

In view of the incompressible flow width scalings in (1), Figs. 7*a* and 8*a* show $(\delta_{1/2}/\vartheta)^2$ plotted against (x/ϑ). If the present supersonic wake follows the same $(x/\vartheta)^{1/2}$ power-law scaling as does its incompressible counterpart, then the symbols in Figs. 7*a* and 8*a* should fall on straight lines, with the slopes being related to the scaling constant c_δ, and the virtual origin (x_0/ϑ) being identifiable by the x-intercept. The open circles denote the visual thickness $\delta_{1/2}(x)$ determined from moments of the lateral profiles through the mean PLMS images in Fig. 2. The squares denote $\delta_{1/2}(x)$ determined from the mean velocity defect profiles $u(y)$ in Fig. 4.

It is apparent from both Figs. 7*a* and 8*a* that the flow width in the near field for both visual and velocity profiles obey for both Mach 2 and 3 cases obey the 1/2-power law scaling. At these comparatively small values of (x/ϑ), the relative Mach numbers $M_r(x)$ in Fig. 6 are large enough for both cases so that any effects of compressibility should be apparent. The fact that the scaling exponents in Figs. 7*a* and 8*a* appear unchanged by compressibility may not be surprising based on experience in the supersonic mixing layer, where compressibility does not affect the power-law scaling, but reduces the scaling constant dramatically when $M_c > 0.2$.

5.1.1. *Mach 2 Case*

The circles in Fig. 7*a* show that the first several points within the base flow region, as expected, decrease with x due to the narrowing effect of the expansion and recompression process. Beyond the recompression zone, the wake widths for the next fifteen points again increase in accordance with the $(x/\vartheta)^{1/2}$ power-law scaling noted above, as is evident from the straight line fit to these points. Regarding the virtual origin in the compressible wake scaling, the circles in Fig 7*a*. give

$$(x_0/\vartheta)_{vis} = -31 . \qquad (5)$$

This apparent downstream shift of the virtual origin relative to the incompressible value of −128 in (4) is not unexpected, given the reduction in wake width created by the expansion and recompression process in the base flow region. Our previous experiment (Nakagawa & Dahm 1999) suggests that the virtual origin would be expected to shift upstream (become more negative) with increasing jet flow rate. At sufficiently high flow rates, (x_0/ϑ) may approach the incompressible value.

The circles in Fig. 7*a* also indicate the scaling constant in the flow width scaling to be

$$c_\delta = 0.39 . \qquad (6)$$

This is remarkable in that it is higher than the value in the incompressible wake in (3*a*), whereas experience in the supersonic mixing layer indicates a reduction in the value of the flow width scaling constant due to compressibility effects. However in most turbulent shear flows the entrainment rate depends on both the growth rate and the velocity defect decay rate. This latter will be examined in §5.2.

While the scaling constant c_δ from the circles in Fig. 7*a* is significantly higher than the value found for any steady wake generator by Wygnanski *et al* (1986), they found that periodic forcing introduced at the wake generator can dramatically increase the scaling constant over the value obtained from the same generator without forcing (see their Table 2). For forced wakes they find

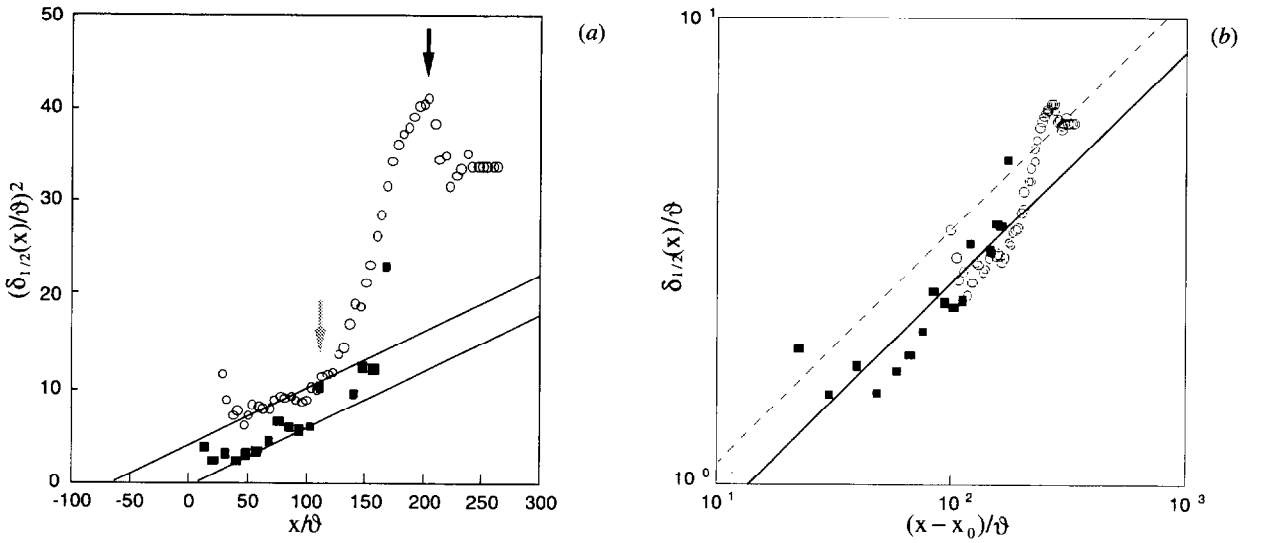

Figure 8. (*a*) Measured flow width $\delta_{1/2}(x)$ for Mach 3 case from mean PLMS intensity profiles in Fig. 2*b* *(circles)* and from mean velocity profiles in Fig. 4*b* *(squares)*. Straight lines show $(\delta/\vartheta) \sim (x/\vartheta)^{1/2}$ scaling, and allow virtual origins and scaling constants to be determined. Profiles are accelerated around $(x/\vartheta) = 110$. The peak of the growth rate at the location near $(x/\vartheta) = 200$ coincide with locations of recompression wave intersections in Fig. 2*b* indicated by an black arrow. The gray arrow indicates the point where the leading characteristics of expansion wave intersects on the center. (*b*) Flow widths $\delta_{1/2}(x)$ from Fig. 8*a* in log-log form, with lines indicating 1/2-power law scaling for values of the far-field scaling constant c_δ in (3) for forced incompressible wakes *(dashed line)* and unforced incompressible wakes *(solid line)* of Wygnanski *et al* (1986).

$$c_\delta = 0.35 \pm 0.03\,, \tag{7}$$

which would appear to be in accord with the present value in (6). It will be seen later in this section that there is a strong likelihood that confined supersonic wakes, such as the present, experience wave-induced periodic forcing due to intersections of the reflected expansion waves with the organized vortical structure of the flow.

The square symbols in Fig. 7*a* also give the same value for the scaling constant, namely $c_\delta = 0.39$ as in (6). Only the virtual origin is different in this case, giving

$$(x_0/\vartheta) = +22\,. \tag{8}$$

As noted above, the downstream shift of the virtual origin relative to the incompressible value is not surprising. The fact that the virtual origin in (5) for the visual widths is more negative than that in (8) for the velocity profile widths appears to be consistent with the common observation that scalar profiles tend to be wider than velocity profiles in turbulent shear flow.

Furthermore, for $(x/\vartheta) \geq 80$, the data for both visual thickness profiles in Fig. 7*a* no longer appear to follow the $(x/\vartheta)^{1/2}$ power-law scaling of the incompressible wake. Yet these far downstream locations are precisely where the reflected expansion waves intersect on the large-scale structures of the wake, while squares in this region are not available due to the interaction reflected recompression wave. This phenomenon will be described in detail later in §5.1.3.

Figure 7*b* shows the mean flow width scalings, in log-log form, with the appropriate value of the virtual origin for the data in Fig. 7*a*. The unforced and forced incompressible wake scalings of Wygnanski *et al* (1986) are also shown for comparison. This summarizes the flow width scaling properties for the Mach 2 case.

5.1.2. *Mach 3 Case*

Considering the virtual origin in the compressible wake scaling for the Mach 3 case, the circles in Fig. 8*a* give

$$(x_0/\vartheta)_{vis} = -90\,, \tag{9}$$

which is similarly shifted downstream from the value for incompressible case due to the existence of the base flow region. The scaling constant in the flow width scaling is found to be

$$c_\delta = 0.26\,. \tag{10}$$

It is now lower than the constant value obtained in the Mach 2 case, and comparable to the value in (3*a*) for the incompressible wake. The difference of these scaling constants for the Mach 2 and Mach 3 cases will be explained also in the next section.

In addition, the squares in Fig. 8*a* give essentially the same slope as that for the circles, indicating the scaling constant, namely $c_\delta = 0.26$ as in (10). Only the virtual origin is different in this case, giving

$$(x_0/\vartheta) = +5\,. \tag{11}$$

The rapid increase in the growth rate from the $(x/\vartheta)^{1/2}$ power-law scaling of the incompressible wake is again observed in Fig. 8*a*, which now begins at around $(x/\vartheta) \geq 100$. For the Mach 3 case, this phenomenon is also seen in the square symbols.

A log-log form of the mean flow width scalings is plotted in Fig.

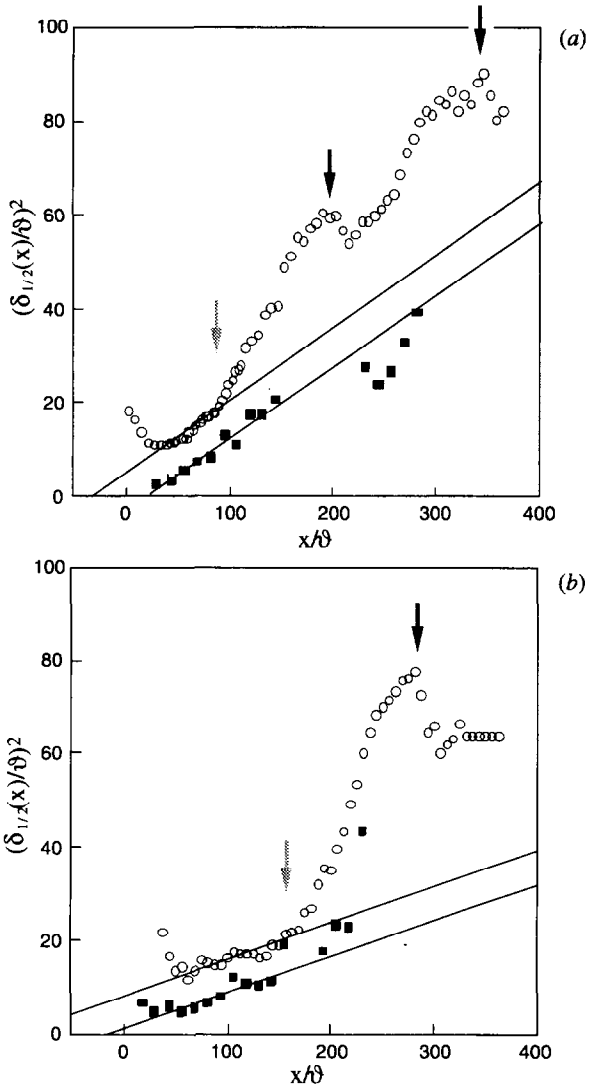

Figure 9. Comparison of Flow widths between (*a*) the Mach 2 case and (*b*) the Mach 3 by using the same $\vartheta = 0.4$ mm. Flow width $\delta_{1/2}(x)$ from mean PLMS image and mean velocity profile with classical $(x/\vartheta)^{-1/2}$ incompressible flow scalings are shown. Departures from the original incompressible scalings are evident in both plots due to self-excited forcing of large-scale structure frequency (*e.g.*, Oster & Wygnanski 1982). Note that the departure points, as indicated by a gray arrow, are shifted significantly downstream in (*b*).

8*b*, along with lines of unforced and forced incompressible wake scalings of Wygnanski *et al* (1986), summarizing our analysis of width scaling properties for Mach 3 case.

5.1.3. *Comparison*

Results for the wake visual and velocity widths in the Mach 2 and Mach 3 cases show that after the compression region the both cases initially follow the classical 1/2-power scaling of incompressible turbulent wakes. The results also showed a dramatic increase in the growth rate further downstream. To understand this phenomenon, it is helpful to replot Fig. 8*a* by using the same ϑ as in the Fig. 7*a* and compare both figures as shown in Fig. 9. (Note that Fig. 9*a* is the same as Fig. 7*a*, and reproduced here to allow direct comparison.) It is essential to mention that the circles for the Mach 2 case in Fig. 9*a* show two strong peaks centered roughly at $(x/\vartheta) \approx 180$ and 330, corresponding respectively to x = 7.2 cm and 13.5 cm as indicated by black arrows. On the other hand, for Mach 3 case in Fig. 9*b* the strong peak is centered roughly at $(x/\vartheta) \approx 280$, corresponding to x = 11.5 cm. These positions coincide with the dark regions in Fig. 2, which in turn coincide with the locations where the reflected recompression shocks intersect the wake flow.

Moreover, as indicated by the gray arrows in Figs. 9*a* and 9*b*, the point at which the growth rate begins rapidly growing is shifted significantly further downstream for the Mach 3 case. These positions are seen at $(x/\vartheta) \approx 80$ for the Mach 2 case and $(x/\vartheta) \approx 160$ for the Mach 3, respectively corresponding to x = 3.2 cm and x = 6.4 cm. Those positions precisely match the locations where the first characteristics of the reflected expansion waves intersect the wake, as seen in Fig. 2. Since the wave angles are shallower for the Mach 3 case, these reflections from the side walls intersect with the wake further downstream, and this is very consistent with our observation above.

These observations suggest that the rapid increase and subsequent decrease in the flow width in Fig. 9 at these locations may be a result of sympathetic interactions between the reflected expansion and shock waves and the quasi-periodic, large-scale, vortical structure of the wake. This mechanism is similar to a phenomenon commonly observed in periodically forced mixing layers (e.g., Oster & Wygnanski 1982). At downstream locations where the forcing frequency closely matches the local natural frequency $u(x)/\delta(x)$ associated with the passing of large-scale structures in the flow, the vortical structures lock onto the forcing frequency. This effect causes the flow width to increase much more rapidly than it normally would as it approaches the point where the natural frequency and the forcing frequency match, and then to remain locked at roughly that width for some distance past this point, before subsequently returning to its natural growth rate.

In the supersonic wake, such periodic forcing could result from the passing of the organized large-scale vortical structures in the wake flow through the reflected expansion waves. As a consequence of this inherently quasi-periodic forcing mechanism, the resulting local forcing frequency due to these waves would automatically be matched to the local natural frequency of the vortical structures. It is presumably this self-excited enforcing mechanism that causes the circles in Figs. 7*a* and 8*a* to depart from the incompressible scaling, given by the lines, at downstream distances.

Additionally, these results also show that the scaling constants for the Mach 2 and Mach 3 cases are apparently different. More precisely, these constants respectively agree with those of forced and unforced of incompressible wake. The possible explanation for this is that for the Mach 2 case, the periodic forcing due to the wave interaction may propagate upstream affecting the scaling constants in the wake near field as well. Any "subsonic path" in the instantaneous Mach number would allow such propagation, while the supersonic mean flow Mach number might appear to preclude upstream propagation of disturbances from this downstream forcing. This phenomenon could happen for the Mach 2 case since the leading characteristic of reflected expansion waves may intersect where the local instantaneous

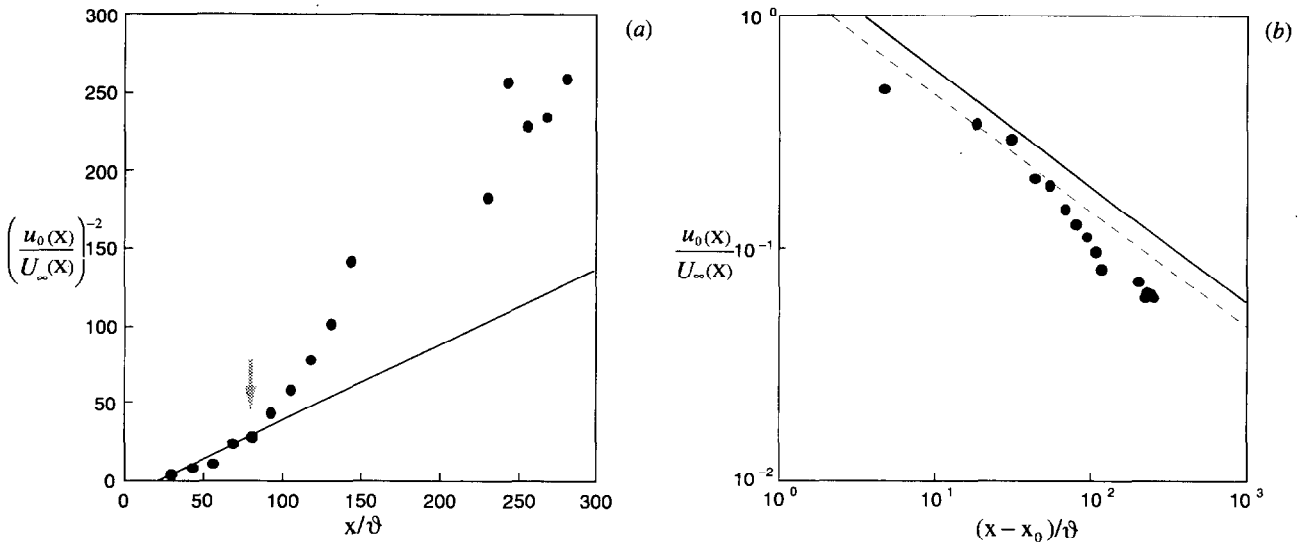

Figure 10. (*a*) Wake centerline defect velocity $u_0(x)$ for the Mach 2 case from velocity profiles in Fig. 4*a* obtained from pressure profiles in Fig. 3. Straight line indicates $(u/U_\infty) \sim (x/\vartheta)^{-1/2}$ scaling, allowing virtual origin and scaling constant to be determined. The gray arrow indicates the point where the leading characteristics of expansion wave intersects on the center. (*b*) Wake centerline defect velocity $u_0(x)$ from Fig. 10*a* in log-log form, with lines indicating −1/2-power law scaling for values of the scaling constant c_u in (2) for the forced incompressible wakes *(dashed line)* and unforced incompressible wakes *(solid line)* of Wygnanski *et al* (1986).

Mach number inside the wake could still be subsonic. On the other hand, for the Mach 3 case, since this intersection occurs further downstream as seen Fig. 9, the local Mach number inside the wake has already been accelerated well into supersonic at the point of intersection; *i.e.*, no subsonic path exists and any forcing information does not propagate upstream before that point.

5.2 Centerline Velocity Defect Scaling *u*(x)

Based on the scaling in (2) for the mean velocity defect in incompressible turbulent wakes noted above, Figs. 10*a* and 11*a* show $(u_0/U_\infty)^{-2}$ plotted against (x/ϑ), where the centerline velocities are determined from measured pitot and static pressures as in Fig. 4. As we have seen in the flow width scalings, if the supersonic wake follows the same $(x/\vartheta)^{-1/2}$ power law scaling as does the incompressible wake, then the symbols in Figs. 10*a* and 11*a* should fall on straight lines, with the slope determining the scaling constants c_u and the virtual origin (x_0/ϑ) identified by the x-intercept.

Over roughly the same downstream region where the flow widths in Figs. 7*a* and 8*a* follow the incompressible scaling, it is again apparent that the centerline velocity defect also follows the −1/2 power-law scaling of the incompressible wake, as indicated by the line in Figs. 10*a* and 11*a*.

For the Mach 2 case, the virtual origin is found in Fig. 10*a* to be

$$(x_0/\vartheta) = +25\,, \qquad (12)$$

in reasonable agreement with the value obtained for the velocity profile widths in (8) from Fig. 7*a*.

The slope of the line in Fig. 10*a* corresponds to a value for the scaling constant of

$$c_u = 1.41\,. \qquad (13)$$

This is somewhat lower than the value of 1.88 in (3*b*) found by Wygnanski *et al* (1986) for unforced, incompressible wakes, however, this value is indeed reasonably close to the value $c_u \approx 1.46 \pm 0.1$ for forced incompressible wake as reported in their Table 2.

Similarly for the Mach 3 case, the virtual origin is found from Fig. 11*a* to be

$$(x_0/\vartheta) = +12\,. \qquad (14)$$

This is also in reasonable agreement with the value in (11), as obtained in Fig. 8*a*. Also the slope of the line in Fig. 11*a* corresponds to a value for the scaling constant of

$$c_u = 2.0\,, \qquad (15)$$

and this is somewhat similar to the value of 1.88 in (3*b*) found by Wygnanski *et al* (1986) for unforced, incompressible, bluff-body wakes.

Figure 12 shows direct comparison of velocity decay scaling for each case by replotting Fig. 11*a* using the same ϑ in Fig. 10*a* as it was similarly done in Fig. 9. Figure 12 shows the point where the velocity defects depart from the line, which indicates the incompressible scaling in the near field, shifts downstream for the Mach 3 case. These points correspond to $(x/\vartheta) \approx 80$ or $x = 3.2$ for Mach 2 case, and $(x/\vartheta) \approx 160$ or $x = 6.4$ for the Mach 3 case and these are consistent with the values we obtained from flow width scalings in Fig. 9. Therefore, this higher velocity decay similarly reflects the increased growth rate caused by

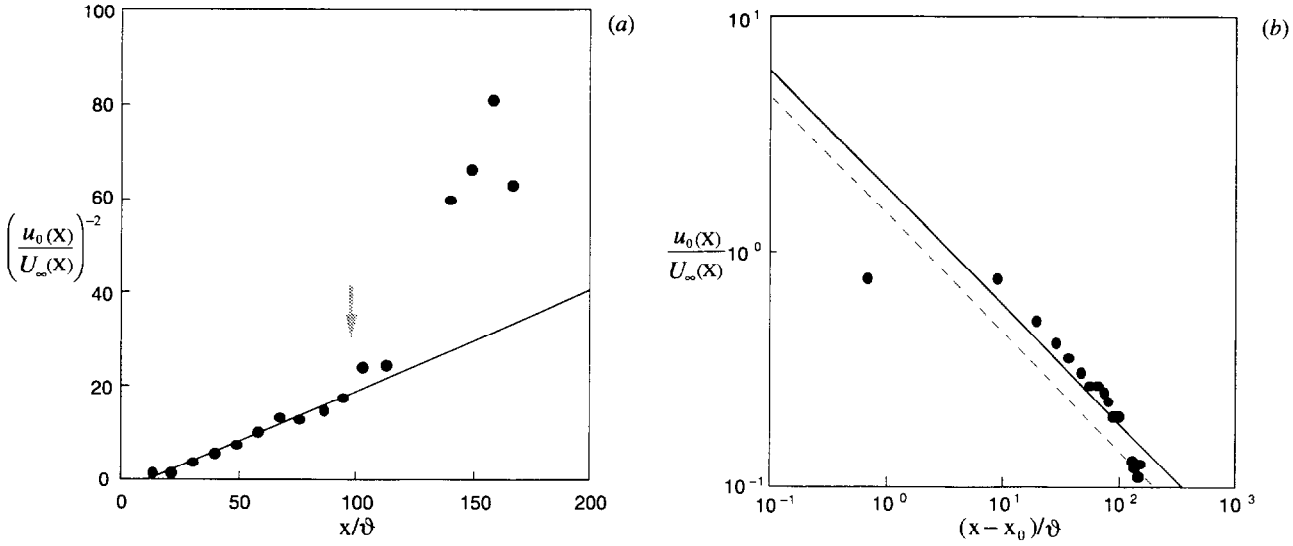

Figure 11. (*a*) Wake centerline defect velocity $u_0(x)$ for the Mach 3 case from velocity profiles in Fig. 4*b* obtained from pressure profiles. Straight line indicates $(u/U_\infty) \sim (x/\vartheta)^{-1/2}$ scaling, allowing virtual origin and scaling constant to be determined. The gray arrow indicates the point where the leading characteristics of expansion wave intersects on the center. (*b*) Wake centerline defect velocity $u_0(x)$ from Fig. 11*a* in log-log form, with lines indicating -1/2-power law scaling for values of the scaling constant c_u in (4) for the forced incompressible wakes *(dashed line)* and unforced incompressible wakes *(solid line)* of Wygnanski *et al* (1986).

incipient locking of the wake vortical structures onto the forcing frequency produced by expansion wave intersection as it was described in detail in §5.1.3.

Figures 10*b* and 11*b* show the centerline mean velocity defect scalings in (13) and (15), in log-log form, for the supersonic turbulent wake, and the unforced and forced scalings of Wygnanski *et al* (1986) are also shown for comparison. These scaling constants are consistent with the results for flow width scalings in Figs. 7*b* and 8*b*.

Combining the results of scaling constants, we could finally find the outer-scale Reynolds number $Re_\delta(x)$ which is independent of x and equal to $Re_\vartheta \cdot c_\delta \cdot c_u$, where Re_ϑ is the Reynolds number based on momentum thickness ϑ and the free stream velocity which is Re_ϑ = 31,000 for the Mach 2 case and 24,000 for the Mach 3 case as shown in Table 1.

6. CONCLUSIONS

Major observations from the present experimental study of Mach number effects on entrainment and mixing in a supersonic, planar, turbulent, bluff-body wake are as follows:

1. In the present supersonic wake the classical vortex street-like large-scale structure of incompressible wakes is recovered in the far field for both Mach 2 and Mach 3 free stream, and the flow widths and mean centerline velocity defects follow the classical $(x/\vartheta)^{1/2}$ and $(x/\vartheta)^{-1/2}$ scalings characteristic of incompressible, planar, turbulent wakes.

2. For Mach 2 case, the measured scaling constants c_δ and c_u in these far field scalings differ significantly from accepted values for unforced, incompressible, planar, turbulent wakes, but agree well with corresponding values for periodically forced incompressible wakes. On the other hand, for Mach 3 case, these constants agree well with values for unforced, incompressible, planar, turbulent wakes. The difference in these scaling constants can be attributed to whether the flow has the "subsonic path" in which forcing information could propagate upstream.

3. The local growth rates of the wake begin growing dramatically at certain points in the downstream regions where the leading characteristic of the reflected expansion waves intersect the flow. This drastic increase in growth rate may be due to a possible quasi-periodic, self-excited, forcing mechanism that results from passage of the organized large-scale vortical structures through the expansion waves. The response of the wake to this local forcing mechanism appears analogous to the response of incompressible mixing layers to periodic forcing.

Collectively in the present study of the supersonic turbulent wake, no clear evidence of compressibility effects was observed in the wake near field immediately after the base flow region where the relative Mach number is relatively large. However, it could be possible that these observation may result from this unique confined geometry in which it is inevitable to have the wave interaction affecting the scaling constants. Moreover, these results also suggest a remarkable mechanism for potentially increasing the growth rates of supersonic turbulent shear flows through judicious control of such expansion wave interactions with the flow. The comparatively strong large-scale structures in two-dimensional, supersonic, turbulent wakes and mixing layers may make these flows particularly suited for such mixing enhancement by self-induced frequency locking of their vortical structures.

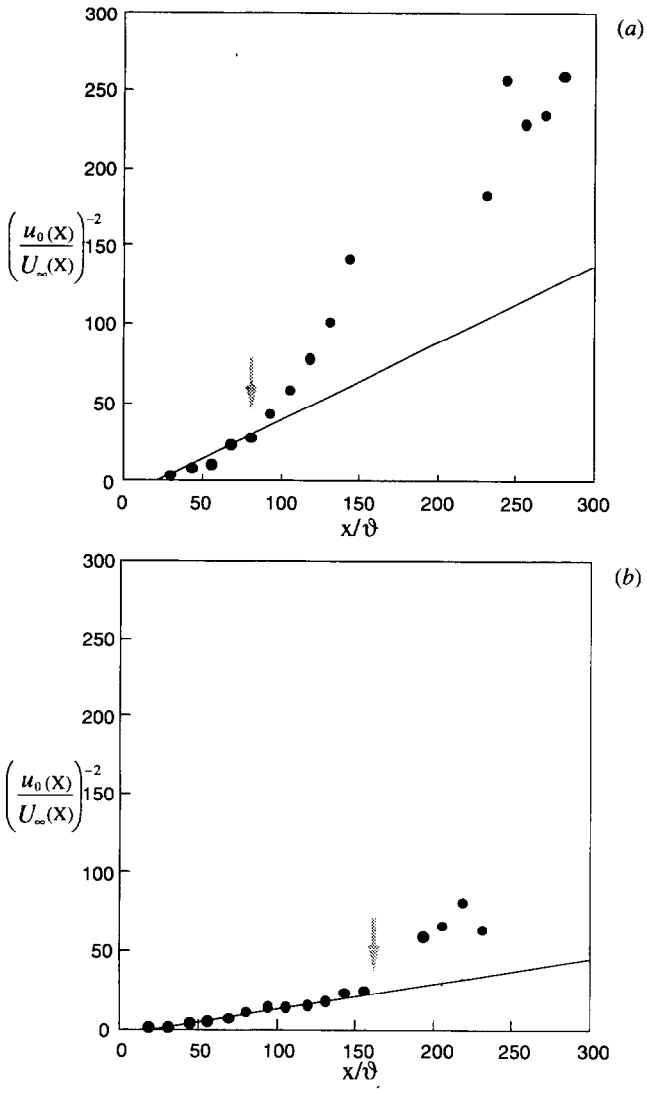

Figure 12. Comparison of velocity defect decay between (*a*) the Mach 2 case and (*b*) the Mach 3 case by using the same $\vartheta = 0.4$ mm. Flow defect centerline velocity profile with classical $(x/\vartheta)^{-1/2}$ incompressible flow scaling are shown. Departure from the original incompressible scaling is evident in both plots due to self-excited forcing of large-scale structure frequency (e.g., Oster & Wygnanski 1982). Note that the departure point, as indicated by the gray arrow, are shifted significantly downstream in (*b*).

Acknowledgements

This work has been supported by the Air Force Office of Scientific Research under AFOSR Grant Nos. F49620-95-1-0115 and F49620-98-1-0003.

References

Amatucci, V.A., Dutton, J.C., Kuntz, D.W. & Addy, A.L. (1992) Two-stream, supersonic, wake flowfield behind a thick base. Part I: General features. *AIAA J.* **30**, 2039-2046.

Chapman, D.R. (1951) An analysis of base pressure at supersonic velocities and comparison with experiment. NACA TN-2137, National Advisory Committee on Aeronautics.

Chen, J.H., Cantwell, B.J. & Mansour, N.N. (1990) The effect of Mach number on the stability of a plane turbulent wake. *Phys. Fluids* A **2**, 984-1004.

Clemens, N.T. & Mungal, M.G. (1995) Large-scale structure and entrainment in the supersonic mixing layer. *J. Fluid Mech.* **284**, 171-216.

Clemens, N.T., Smith, M.F. & Fernandez, J.V. (1996) Observations of supersonic flat plate wake transition. *AIAA Paper No. 96-0785*, 34th Aerospace Sciences Meeting, AIAA, Washington, D.C.

Clemens, N.T. & Smith, M.F. (1998) Observations of supersonic flat plate wake transition. *AIAA J.* **36**, 1328-1330.

Crookson, R.A., Flanagan, P. and Penny, G.S. (1969) A study of free-jet and enclosed supersonic diffusion flames. *Proc. 12th Int'l Symp. Comb.* 1115-1124, The Combustion Institute, Pittsburgh.

Dimotakis, P.E. (1991) Turbulent free shear layer mixing and combustion. In High-Speed Flight Propulsion Systems (S.N.B. Murthy & E.T. Curran, Eds.) Vol. 137 of Progress in Aeronautics & Astronautics, AIAA, Washington, D.C., 265-340.

Herrin, J.L. & Dutton, J.C. (1994) Supersonic base flow experiments in the near wake of a cylindrical after body. *AIAA J.* **32**, 77-83.

Lachney, E.R. & Clemens, N.T. (1998) PLIF imaging of mean temperature and pressure in a supersonic bluff wake. *Expts. Fluids* **24**, 354-363.

Lachney, E.R., Smith, M.F. & Clemens, N.T. (1995) Laser 2-D imaging of a compressible flat plate wake. *AIAA Paper No. 95-2220*, 26th AIAA Fluid Dynamics Conference, AIAA, Washington, D.C.

Nakagawa, M. & Dahm, W.J.A. (1999) Compressibility effects on entrainment and mixing in supersonic planar turbulent wakes. *AIAA Paper No. 99-3582*, 30th AIAA Fluid Dynamics Conference, AIAA, Washington, D.C.

Nakagawa, M. & Dahm, W.J.A. (1999) Entrainment and mixing in supersonic planar turbulent wakes. *Bull. Am. Phys. Soc.* **44** (8), 171 (abstract only)

Nejad, A.S., Glawe, D.D., Donbar, J.M., Sekar, B, Samimy, M. & Driscoll, J.F. (1994) Parallel fuel injection from the base of an extended strut into supersonic flow; *AIAA Paper No. 94-0711*, AIAA, Washington, D.C.

Northam, G.B., Greenburg, I. & Byington, C.S. (1989) Evaluation of parallel injector configurations for supersonic combustion. *AIAA Paper No. 89-2525*, AIAA, Washington, D.C.

Oster, D. & Wygnanski, I. (1982) The forced mixing layer between parallel streams. *J. Fluid Mech.* **123**, 91-130.

Pope, A. & Goin, K.L. (1965) High-Speed Wind Tunnel Testing. John Wiley & Sons, New York.

Wygnanski, I., Champagne, F. & Marasli, B. (1986) On the large-scale structures in two-dimensional, small-deficit, turbulent wakes. *J. Fluid Mech.* **168**, 31-71.